

THREE-DIMENSIONAL GRAVITY INSTABILITY
DERIVED FROM TWO-DIMENSIONAL
SOLUTIONS

BY
M. A. BIOT

Reprinted for private circulation from
GEOPHYSICS
Vol. XXXI, No. 1, February, 1966

THREE-DIMENSIONAL GRAVITY INSTABILITY DERIVED FROM TWO-DIMENSIONAL SOLUTIONS†

M. A. BIOT*

The theory of three-dimensional gravity instability of multilayers is developed with particular application to salt structures. It is shown that three-dimensional solutions are immediately obtained without further numerical work from the solution of the corresponding two-dimensional problem. Application to a number of typical three-dimensional structures yields the characteristic distance between peaks and crests and shows that this distance does not differ significantly from the wavelength of the two-dimensional solution. Various periodic patterns are examined corresponding to rectangular and hexagonal cells. The time history of nonperiodic structures corresponding to initial deviations from perfect horizontality is also derived. The method is applied to the three-dimensional problem of generation of salt structures when the time-history of sedimentation is taken into account with variable thickness and compaction of the overburden and establishes the general validity of the geological conclusions derived from the previous two-dimensional treatment of the same problem (Biot and Odé, 1965). The present method of deriving three-dimensional solutions, which is developed here in the special context of gravity instability, is valid for a wide variety of problems in theoretical physics.

I. INTRODUCTION

It is now generally accepted that the physical mechanism for the generation of salt domes is provided by the gravity instability which arises when a denser material lies on top of the salt layer. Due to the action of gravity and the plastic properties of the materials the salt tends to intrude into the denser overburden. This mechanism was originally proposed by Arrhenius (1912). Extensive model tests by Nettleton (1934) and evaluation of the scaling factor by Hubbert (1937) with application to actual geological structures and known geological time-scales have put the theory on a firm basis.

Additional model studies and further comparison with geological data have also been made by Dobrin (1941), Parker and McDowell (1955), and Nettleton (1955).

When attempting to develop a mathematical analysis of the generation of salt domes one should distinguish between two phases. The first phase involves the formation of what is sometimes referred to as "pillows" where the upper boundary of the salt structure is deformed in hills and valleys of gentle slope. In the second phase cylindrical columns of salt intrude vertically into the overburden. The cylindrical column (diapir) represents the salt dome proper.

The interest in considering the first phase as a distinct problem lies in the possibility of linearizing the equations. In particular it is justified to consider small perturbations of the medium near a state of hydrostatic equilibrium where the initial stress is approximately isotropic. In the perturbed state the slope of the interfaces between layers remains small and small incremental stresses are generated which are approximately linear functions of the strain rate. This implies that the motion is nearly the same as if the materials were purely viscous. Hence, in spite of the fact that the rheological properties of rock for large strain are strongly nonlinear, we may, in this case, apply the linear equations for viscous fluids using a "differential viscosity" coefficient defined for incremental stresses (Biot, 1961; 1965a, page 390).

It should be noted that, even if we assume a *plastic material* such that under geological conditions creep becomes negligible below a certain threshold of shear stress, the viscous and viscoelastic model will still be valid for *incremental deformations* superposed upon an initial state of slow creep which itself may be due to tectonic action or uneven sedimentation.

Except perhaps insofar as it may clarify certain initiating conditions, the present analysis as well as the earlier two-dimensional treatments

† Manuscript received by the Editor April 23, 1965.

* Consultant, Shell Development Company, New York, New York.

(Biot, 1959, 1963; Biot and Odé, 1965) are not intended to cover the diapir generation which represents the second phase.

The foundation of a mathematical theory of gravity instability applicable to the first phase of salt-dome generation has been established in some earlier work (Biot, 1959, 1960, 1963). It is based on the author's analog model which leads to considerable simplification in the analysis. The effect of gravity is obtained by applying "buoyancy forces" to a gravity-free model. The model is also useful in more complex problems by providing an intuitive understanding of the mechanics.

Completely general analytical solutions and computational schemes have been developed by the author (1963, 1965a) for gravity instability of structures with any number of layers of isotropic or anisotropic materials.

As regards the analog model it should be noted that its validity is not restricted to the first phase of gravity instability. It has been extended to large deformations (Biot, 1965a, 1965b). Also it does not require the medium to be viscous. Hence it is applicable to the second phase and the formation of the salt dome proper. However, in this case more complex rheological properties have to be considered.

As a preliminary to a more elaborate analysis of salt structures the problem of gravity instability was solved for two typical configurations (Biot, 1963). In one configuration the salt layer lies on a rigid base with an infinite viscous overburden. In the other the rigid base is replaced by a deep viscous medium. The results demonstrated the existence of a *dominant wavelength of magnitude compatible with geological data*. The two problems are also discussed in the author's book (1965a, p. 460-465).

These preliminary results justify the validity of assuming a rigid base as a first approximation and provided the foundation for an extension of the analysis to a salt layer with a finite overburden including a time-dependent thickness and compaction (Biot and Odé, 1965). The purpose of that paper was twofold: First to bring out and isolate the controlling nondimensional parameters of geological significance, second, having done this, to use the insight gained to derive a simple and manageable analysis of the much more complex problem where the thickness of the overburden is

a function of time and its compaction function of time and depth. In the course of this analysis the effect of surface erosion has also been evaluated. The theory is therefore valid for the geologically more realistic case where the time-history of sedimentation is taken into account. The numerical results derived from this theory are in general agreement with geological data and with the geological time-scale.

Dominant wavelengths are not sensitive to physical properties. Hence they may be predicted with fair reliability in spite of the lack of accurate data on rock properties. However, this is not true for the time history for which *only orders of magnitudes* may be compared with accepted geological time-scales.

The two-dimensional analysis carried out in the aforementioned papers yields the quantitatively significant physical features. However, it is of interest to evaluate more precisely the correction factors which must be applied in order to extend the results to problems of three-dimensional instability.

It is the purpose of this paper to derive very general three-dimensional solutions and to show that they can be obtained immediately in numerical form from the solution of the corresponding two-dimensional problem by a method of superposition without having to perform any new computations. The method is valid for the three-dimensional problem with any number of layers including the case where the time-history of sedimentation and compaction is taken into account. In fact, it is not restricted to these particular applications and may be used in a large class of other problems in applied mathematics.

These three-dimensional solutions correspond to a deformation of the salt-overburden interface which forms a pattern of hills, hollows, crests, and valleys. Periodic patterns correspond to rectangular or hexagonal cells. A particular nonperiodic pattern is represented by a structure with circular contour lines. We will show how the latter result may be used to estimate the type of pattern that builds up gradually as a result of irregular initial deviations of the interface from a perfect horizontal plane. Numerical results are also discussed for various patterns in the case of an overburden with variable thickness and compaction.

The present analysis leads to the conclusion that in the three-dimensional pattern the char-

The rotated pattern (2.3) is also a solution of the problem of instability.

The same considerations are of course also applicable to a horizontal translation of the pattern.

As will now be shown, these methods of superposition and rotation lead to a completely general analysis of three-dimensional instability by using as basic components the two-dimensional solutions.

The procedure is evidently applicable to a much wider range of problems than those of gravity instability which are considered below since the only condition required is that of transverse isotropy and the validity of the superposition principle.

3. BASIC TWO-DIMENSIONAL SOLUTIONS

The two-dimensional solutions of gravity instability which we shall use as basic components to build up three-dimensional solutions were derived in previous papers (Biot, 1960, 1963; Biot and Odé, 1965). These solutions assume a sinusoidal distribution along the horizontal x direction and are independent of y . Hence they are of the form

$$W = f(z)e^{pt} \cos lx. \quad (3.1)$$

Note that in the aforementioned papers the vertical axis was denoted by y instead of z . The vertical distribution function depends on the wavelength. This dependence is not relevant at this point and we shall come back to it later.

The solution (3.1) amounts to putting

$$w(x, y) = \cos lx \quad (3.2)$$

in the general expression (2.1). Hence in this two-dimensional case the deformation pattern of a typical interface is a cylindrical surface with sinusoidal corrugations.

For brevity, a pattern of the type (3.2) corresponding to a two-dimensional solution will be referred to hereafter as a *sinusoidal pattern*.

The wavelength or distance between crests is

$$\mathcal{L} = \frac{2\pi}{l}. \quad (3.3)$$

The sinusoidal pattern may be translated arbitrarily in the horizontal plane. This amounts to

adding an arbitrary phase to the sinusoidal pattern. Hence we may also express it as

$$w(x, y) = \sin lx, \quad (3.4)$$

or, in the more general form,

$$w(x, y) = \sin (lx + \theta), \quad (3.5)$$

with an arbitrary phase angle θ .

As pointed out in the previous section, the pattern may also rotate about a vertical axis. According to equation (2.3) the rotation amounts to replacing lx by

$$lx' = l(x \cos \alpha + y \sin \alpha), \quad (3.6)$$

where α is the angle of rotation (Figure 1).

By putting

$$\begin{aligned} \xi &= l \cos \alpha, \\ \eta &= l \sin \alpha, \end{aligned} \quad (3.7)$$

the sinusoidal patterns (3.2), (3.4), and (3.5) after rotation become

$$\begin{aligned} w(x, y) &= \cos (\xi x + \eta y), \\ w(x, y) &= \sin (\xi x + \eta y), \\ w(x, y) &= \sin (\xi x + \eta y + \theta). \end{aligned} \quad (3.8)$$

Note that

$$l = \sqrt{\xi^2 + \eta^2}. \quad (3.9)$$

It is also convenient to express these results vectorially by using a coordinate vector,

$$\mathbf{r} = (x, y), \quad (3.10)$$

and a unit vector,

$$\mathbf{n} = (\cos \alpha, \sin \alpha). \quad (3.11)$$

The latter points in a direction rotated clockwise through an angle α from the x direction. The rotated sinusoidal patterns (3.8) become

$$\begin{aligned} w(x, y) &= \cos (\mathbf{l n} \cdot \mathbf{r}), \\ w(x, y) &= \sin (\mathbf{l n} \cdot \mathbf{r}), \\ w(x, y) &= \sin (\mathbf{l n} \cdot \mathbf{r} + \theta). \end{aligned} \quad (3.12)$$

The coefficient p appearing in the exponential factor $\exp (pt)$ determines the rate of growth of the altitude of the crests for a particular wave-

length. It is a function of the wavelength. Hence, we write

$$p = p(l). \quad (3.13)$$

In general, there is a value l_d of l for which p acquires a maximum value

$$p_m = p(l_d). \quad (3.14)$$

The corresponding wavelength is

$$\mathcal{L}_d = \frac{2\pi}{l_d}. \quad (3.15)$$

We have referred to \mathcal{L}_d as the *dominant wavelength* because it tends to predominate after certain time during the process of growth of an initially irregular configuration.

4. RECTANGULAR PATTERN

Consider the first of the sinusoidal patterns (3.8) obtained by rotation through an angle α

$$w_1(x, y) = \cos(\xi x + \eta y). \quad (4.1)$$

Another pattern is obtained by changing the sign of α

$$w_2(x, y) = \cos(\xi x - \eta y). \quad (4.2)$$

By superposition, the sum of expressions (4.1) and (4.2) yields a pattern w which represents a three-dimensional instability. We derive

$$w(x, y) = w_1 + w_2 = 2 \cos \xi x \cos \eta y. \quad (4.3)$$

In this pattern the nodal lines ($w=0$) form a rectangular network. Adjacent rectangular areas are regions of upward and downward displacements. Lengths of the sides of a rectangular hill are

$$\begin{aligned} a &= \pi/\xi, \\ b &= \pi/\eta. \end{aligned} \quad (4.4)$$

Note that we have superposed two sinusoidal patterns of the *same wavelength* $\mathcal{L} = 2\pi/l$. Hence the height and depth of the rectangular pattern grows proportionally to the exponential factor $\exp(pt)$ where $p(l)$ is a function of the wavelength of the corresponding two-dimensional solution. In terms of the size of the rectangle this wavelength is [computed from equations (3.7) and (4.4)]

$$\mathcal{L} = \frac{2\pi}{l} = \frac{2ab}{\sqrt{a^2 + b^2}}. \quad (4.5)$$

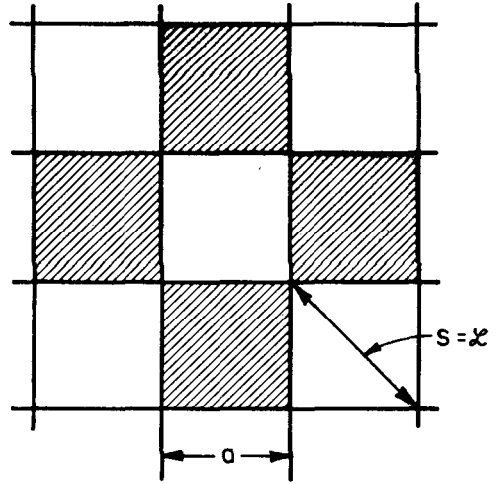


FIG. 2. Square pattern. Shortest distance between peaks is $S = \mathcal{L}$. In this figure and others below, hills are indicated by blank areas, hollows by shaded areas.

There is an infinity of rectangular shapes corresponding to the same wavelength, \mathcal{L} , and the same rate of growth as can be seen by varying the ratio a/b in equation (4.5). The case of a square pattern ($a=b$) is illustrated in Figure 2. In this figure and the following ones blank and shaded areas represent, respectively, hills and hollows.

For a square pattern equation (4.5) becomes

$$\mathcal{L} = \sqrt{2} a. \quad (4.6)$$

In this case the shortest distance, S , between peaks is equal to the diagonals $\sqrt{2}a$ of the squares. Hence

$$S = \mathcal{L}. \quad (4.7)$$

This shows that for the square pattern the characteristic distance, S , between peaks is equal to the wavelength, \mathcal{L} , of the corresponding two-dimensional solution. For hills and hollows of maximum rate of growth, S is equal to the dominant wavelength, \mathcal{L}_d , of the corresponding two-dimensional problem.

5. CIRCULAR PATTERN

The same procedure of superposition may be used to derive a pattern with circular contour lines, represented by Bessel functions. This is obtained by superposing an infinite number of sinusoidal patterns

$$w(x, y) = \cos(\mathbf{l} \cdot \mathbf{r}), \quad (5.1)$$

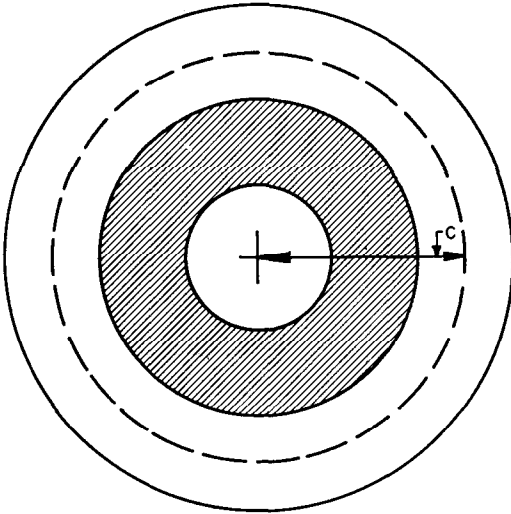


FIG. 3. Circular pattern. Characteristic distance of the central peak to the first crest is $C = 1.116\mathcal{L}$.

with equal amplitude and wavelength oriented isotropically about a vertical axis. The result amounts to an integration with respect to the angle α , and is written

$$w(x, y) = \int_0^{2\pi} \cos(\mathbf{l}\mathbf{n} \cdot \mathbf{r}) d\alpha. \tag{5.2}$$

The integral may be transformed by introducing polar coordinates, putting

$$\begin{aligned} x &= r \cos \phi, \\ y &= r \sin \phi, \end{aligned} \tag{5.3}$$

hence

$$\mathbf{n} \cdot \mathbf{r} = r \cos(\alpha - \phi). \tag{5.4}$$

With the variable $\beta = \alpha - \phi$ and because the integration is performed over a complete period 2π the integral (5.2) is equivalent to the form

$$\begin{aligned} w(x, y) &= \int_0^{2\pi} \cos[lr(\cos \beta)] d\beta \\ &= \int_0^{2\pi} e^{ilr \cos \beta} d\beta. \end{aligned} \tag{5.5}$$

The value of this integral is well known in terms of Bessel's function.¹ We derive

$$w(x, y) = 2\pi J_0(lr). \tag{5.6}$$

¹ See, for example, McLachlan (1934), page 43.

Thus the pattern is represented by circular contour lines (Figure 3). A central hill is surrounded by concentric crests and valleys.

The characteristic distance C of the center to the nearest circular crest is found by using tables of Bessel functions. This leads to the value

$$lC = 7.016. \tag{5.7}$$

Hence

$$C = 1.116\mathcal{L}. \tag{5.8}$$

This value is slightly larger than the wavelength, \mathcal{L} , of the two-dimensional solution. As we move further away from the center the solution approaches the two-dimensional case and the distance between circular crests tends toward the wavelength, \mathcal{L} .

Again there is a characteristic distance

$$C = 1.116\mathcal{L}_d, \tag{5.9}$$

for which the rate of growth is maximum. This value is determined by the dominant wavelength, \mathcal{L}_d , of the corresponding two-dimensional problem.

The same conclusions apply, of course, to the circular pattern obtained by reversing the sign of the elevation w . In this case the central hill is replaced by a hollow and crests are replaced by valleys.

6. TRIANGULAR PATTERN

By using the same process of superposition it is possible to derive a periodic pattern where the nodal lines form a network of equilateral triangles. To show this we make use of the second of equations (3.12),

$$w(x, y) = \sin(\mathbf{l}\mathbf{n} \cdot \mathbf{r}). \tag{6.1}$$

We choose three unit vectors $\mathbf{n}_1, \mathbf{n}_2, \mathbf{n}_3$ in directions which differ by 120 degrees (Figure 4). By adding the three corresponding expressions (6.1) we obtain

$$\begin{aligned} w(x, y) &= \sin(\mathbf{l}\mathbf{n}_1 \cdot \mathbf{r}) + \sin(\mathbf{l}\mathbf{n}_2 \cdot \mathbf{r}) \\ &\quad + \sin(\mathbf{l}\mathbf{n}_3 \cdot \mathbf{r}). \end{aligned} \tag{6.2}$$

This is a three-dimensional pattern which results from the superposition of three sinusoidal patterns whose nodal lines are oriented at 120 degrees from each other.

A cyclic permutation of $\mathbf{n}_1, \mathbf{n}_2, \mathbf{n}_3$ leaves expres-

sion (6.5) unchanged; hence the pattern is invariant for any rotation of 120 degrees.

In order to show that the nodal lines form equilateral triangles, we make use of the trigonometric identity

$$\begin{aligned}
 4 \sin X_1 \sin X_2 \sin X_3 &= -\sin(X_1 + X_2 + X_3) \\
 &+ \sin(-X_1 + X_2 + X_3) \\
 &+ \sin(X_1 - X_2 + X_3) \\
 &+ \sin(X_1 + X_2 - X_3). \quad (6.3)
 \end{aligned}$$

Since they are oriented symmetrically, the three unit vectors satisfy the following relations,

$$\begin{aligned}
 \mathbf{n}_1 + \mathbf{n}_2 + \mathbf{n}_3 &= 0, \\
 \frac{1}{2}(-\mathbf{n}_1 + \mathbf{n}_2 + \mathbf{n}_3) &= -\mathbf{n}_1, \\
 \frac{1}{2}(\mathbf{n}_1 - \mathbf{n}_2 + \mathbf{n}_3) &= -\mathbf{n}_2, \\
 \text{and } \frac{1}{2}(\mathbf{n}_1 + \mathbf{n}_2 - \mathbf{n}_3) &= -\mathbf{n}_3. \quad (6.4)
 \end{aligned}$$

We put

$$\begin{aligned}
 -X_1 &= \frac{1}{2}l\mathbf{n}_1 \cdot \mathbf{r} & -X_2 &= \frac{1}{2}l\mathbf{n}_2 \cdot \mathbf{r} \\
 -X_3 &= \frac{1}{2}l\mathbf{n}_3 \cdot \mathbf{r}, \quad (6.5)
 \end{aligned}$$

and substitute these values in the trigonometric identity (6.3). Taking into account relations (6.4) we find that the pattern (6.2) may be written in the form

$$\begin{aligned}
 w(x, y) &= -4 \sin\left(\frac{1}{2}l\mathbf{n}_1 \cdot \mathbf{r}\right) \sin\left(\frac{1}{2}l\mathbf{n}_2 \cdot \mathbf{r}\right) \\
 &\cdot \sin\left(\frac{1}{2}l\mathbf{n}_3 \cdot \mathbf{r}\right). \quad (6.6)
 \end{aligned}$$

The nodal lines are those for which $w=0$; hence they are represented by the equations

$$\begin{aligned}
 \frac{1}{2}l\mathbf{n}_1 \cdot \mathbf{r} &= k_1\pi, \\
 \frac{1}{2}l\mathbf{n}_2 \cdot \mathbf{r} &= k_2\pi, \\
 \frac{1}{2}l\mathbf{n}_3 \cdot \mathbf{r} &= k_3\pi, \quad (6.7)
 \end{aligned}$$

where k_1, k_2, k_3 are either zero, positive, or negative integers. They form a network of equilateral triangles.

It is convenient to consider a particular set of unit vectors such that \mathbf{n}_1 is oriented along the x axis. The components of these vectors are then

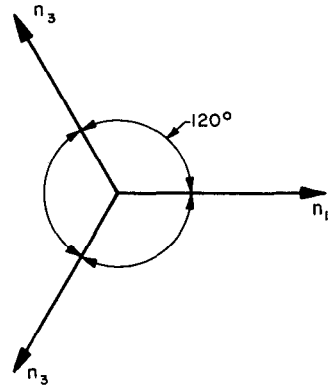


FIG. 4. Unit vectors used to represent the triangular and hexagonal patterns.

$$\begin{aligned}
 \mathbf{n}_1 &= (1, 0), \\
 \mathbf{n}_2 &= \left(-\frac{1}{2}, \frac{\sqrt{3}}{2}\right), \\
 \text{and } \mathbf{n}_3 &= \left(-\frac{1}{2}, -\frac{\sqrt{3}}{2}\right). \quad (6.8)
 \end{aligned}$$

The nodal lines for this case are shown in Figure 5. The pattern is composed of triangular hills and hollows represented by blank and shaded areas, respectively.

That the pattern is also periodic is immediately evident by writing explicitly

$$\begin{aligned}
 \mathbf{n}_1 \cdot \mathbf{r} &= x, \\
 \mathbf{n}_2 \cdot \mathbf{r} &= -\frac{1}{2}x + \frac{\sqrt{3}}{2}y, \\
 \text{and } \mathbf{n}_3 \cdot \mathbf{r} &= -\frac{1}{2}x - \frac{\sqrt{3}}{2}y. \quad (6.9)
 \end{aligned}$$

Referring to equation (6.2) we verify that for a given value of y the pattern remains unchanged by translating it through a distance $4\pi/l = 2\mathcal{L}$ in the x direction. Hence in the x direction it has a period equal to twice the wavelength, \mathcal{L} , of the corresponding sinusoidal pattern. Because of symmetry the same period applies in directions obtained by repeated rotations of 60 degrees.

The periods in the x and y directions are different. Expression (6.2) shows that in the y direction the pattern has a period

$$H = \frac{4\pi}{\sqrt{3}} \frac{1}{l} = \frac{2}{\sqrt{3}} \mathcal{L} = 1.155\mathcal{L}. \quad (6.10)$$

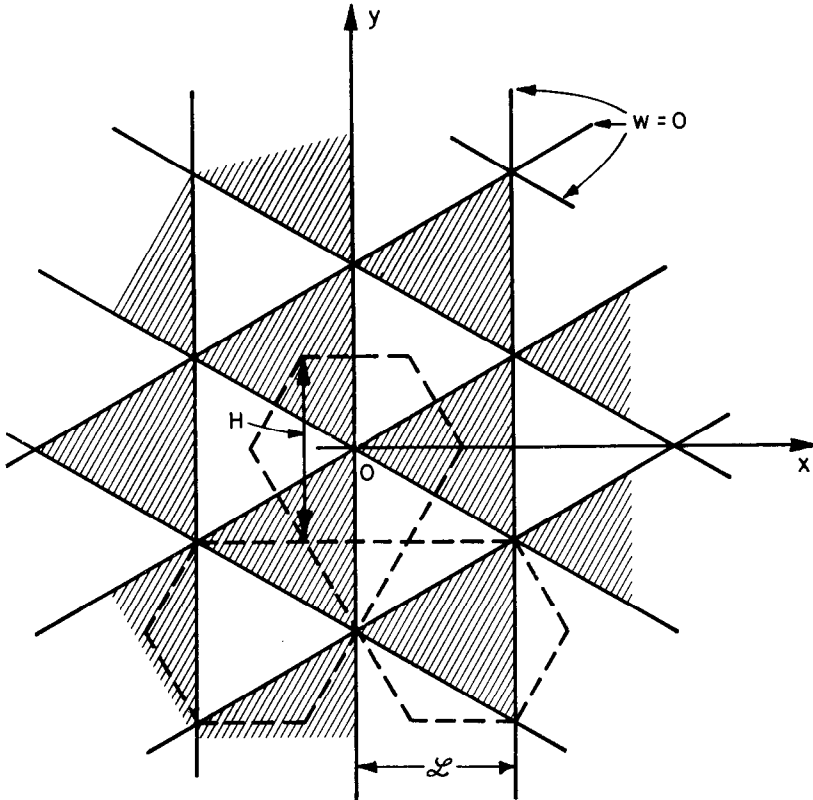


FIG. 5. Triangular pattern showing nodal lines ($w=0$) and corresponding hexagonal cells. Characteristic distance between peaks is $H=1.155\mathcal{L}$.

This period is also equal to the sides of the triangles and represents the shortest distance between peaks. Note that the peaks must lie on axes of symmetry of the pattern and therefore must be located at the center of gravity of the triangles.

As shown by the dotted lines in Figure 5, we may distinguish three types of hexagonal cells indicated by the dotted lines. One is centered on the intersection of the nodal lines and the other two are centered on a peak and a bottom point. The last two are interchanged by a change of sign of the elevation w . Either one of the three cells may be used to construct the periodic pattern. Note that the cell is hexagonal but the symmetry inside is triangular.

If we consider triangular patterns of all possible sizes the one with fastest rate of growth is obtained from the corresponding two-dimensional solution of dominant wavelength \mathcal{L}_d . Equation (6.10) shows that the characteristic distance H

between peaks in this case is about 15 percent higher than the dominant wavelength.

7. HEXAGONAL PATTERN

Let us again superpose three sinusoidal patterns whose nodal lines are oriented at 120 degrees from each other. However, in this case, instead of using the sine functions which led to the previous triangular pattern, we choose the cosine function (5.1). We write

$$w(x, y) = \cos(\mathbf{l}\mathbf{n}_1 \cdot \mathbf{r}) + \cos(\mathbf{l}\mathbf{n}_2 \cdot \mathbf{r}) + \cos(\mathbf{l}\mathbf{n}_3 \cdot \mathbf{r}). \tag{7.1}$$

The unit vectors, $\mathbf{n}_1, \mathbf{n}_2, \mathbf{n}_3$ are the same as those shown in Figure 4. They satisfy relations (6.4).

The patterns (6.2) and (7.1) differ by the phasing of the three sinusoidal components. In equation (6.2) three nodal lines intersect at the same point, while equation (7.1) represents the sum of

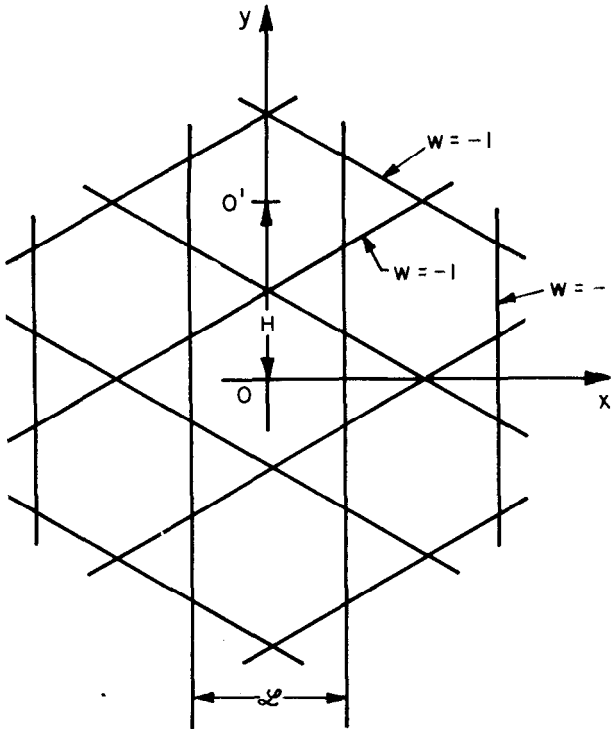


FIG. 6. Network of contour lines of elevation $w = -1$ for the hexagonal pattern.

sinusoidal patterns whose crest lines intersect at the same point.

The pattern (7.1) remains unchanged under cyclic permutation of $\mathbf{n}_1, \mathbf{n}_2, \mathbf{n}_3$, hence for any rotation of 120 degrees. In addition, it remains unchanged when the unit vectors are changed in sign. This amounts to an inversion. These two operations are seen to be equivalent to a 60-degree rotation. Hence the pattern possesses hexagonal symmetry.

In order to obtain a clearer picture of the geometry we use the following trigonometric identity

$$\begin{aligned}
 &4 \cos X_1 \cos X_2 \cos X_3 \\
 &= \cos (X_1 + X_2 + X_3) \\
 &+ \cos (-X_1 + X_2 + X_3) \\
 &+ \cos (X_1 - X_2 + X_3) \\
 &+ \cos (X_1 + X_2 - X_3). \quad (7.2)
 \end{aligned}$$

By substituting the values (6.5) for X_1, X_2, X_3 , and taking into account relations (6.4), we find that the pattern (7.1) may be written

$$\begin{aligned}
 w(x, y) = &4 \cos \left(\frac{1}{2}\mathbf{n}_1 \cdot \mathbf{r}\right) \cos \left(\frac{1}{2}\mathbf{n}_2 \cdot \mathbf{r}\right) \\
 &\cdot \cos \left(\frac{1}{2}\mathbf{n}_3 \cdot \mathbf{r}\right) - 1. \quad (7.3)
 \end{aligned}$$

This expression shows that the contour lines of altitude $w = -1$ are the straight lines

$$\begin{aligned}
 \frac{1}{2}\mathbf{n}_1 \cdot \mathbf{r} &= \left(k_1 + \frac{1}{2}\right)\pi, \\
 \frac{1}{2}\mathbf{n}_2 \cdot \mathbf{r} &= \left(k_2 + \frac{1}{2}\right)\pi, \\
 \frac{1}{2}\mathbf{n}_3 \cdot \mathbf{r} &= \left(k_3 + \frac{1}{2}\right)\pi, \quad (7.4)
 \end{aligned}$$

where k_1, k_2, k_3 are either zero, positive, or negative integers. These lines form a periodic network of hexagons and triangles shown in Figure 6.

The peaks of elevation $w = 3$ are located at the centers such as o and o' of hexagons in Figure 6. The distance oo' between peaks is obtained as follows. With the values (6.8) for $\mathbf{n}_1, \mathbf{n}_2, \mathbf{n}_3$, we substitute $x = 0$ into expression (7.1). It becomes

$$w(0, y) = 1 + 2 \cos \left(\frac{\sqrt{3}}{2}ly\right). \quad (7.5)$$

The period of this expression along y represents the shortest distance between peaks. Its value is

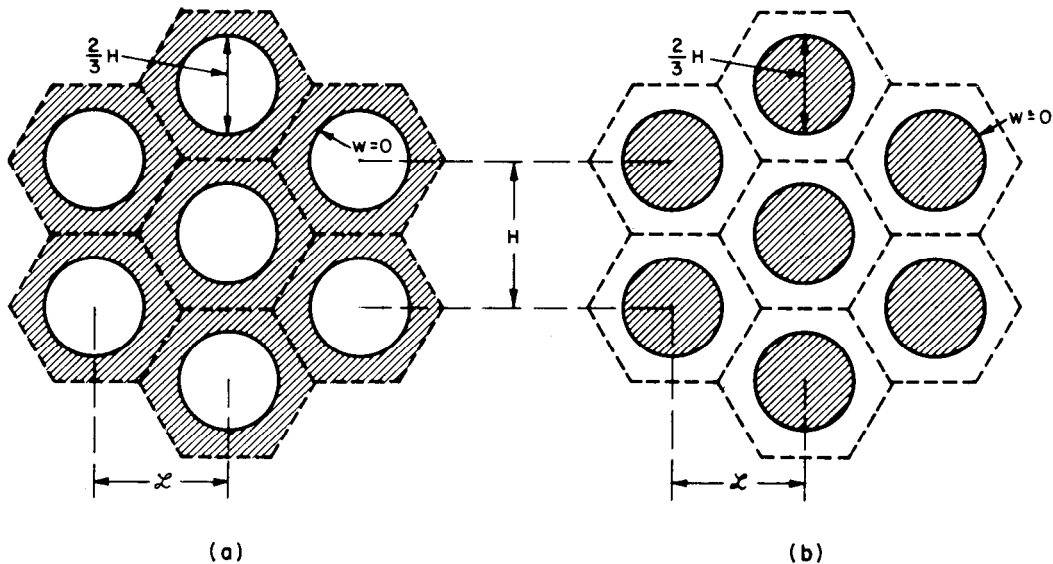


FIG. 7. Hexagonal patterns, showing nodal lines, and corresponding hexagonal cells. (a) Hills separated by a network of valleys; (b) hollows separated by a network of crests. Characteristic distance between peaks is $H = 1.155L$.

$$H = \frac{4\pi}{\sqrt{3}} \frac{1}{l} = 1.155L. \quad (7.6)$$

It is the same as the characteristic distance (6.10) for the triangular pattern.

The nodal line lies inside the hexagon and is almost circular. The ordinate y_0 at which it intersects the y axis is found by putting $w=0$ in equation (7.5). We find

$$y_0 = \frac{1}{3} \frac{4\pi}{\sqrt{3}} \frac{1}{l} = \frac{1}{3} H. \quad (7.7)$$

Two main patterns are derived. The one shown in Figure 7a is composed of near circular hills separated by a hexagonal network of valleys. Changing the sign of the elevation w yields the pattern of Figure 7b where near circular hollows are separated by a hexagonal network of crests as indicated in the figure.

We may also distinguish hexagonal cells of the same size as those of the triangular pattern of section 6.

8. GENERALIZED PATTERNS

Patterns corresponding to three-dimensional solutions of a very general type are obtained by superposition of sinusoidal components. We write

$$w(x, y) = \sum_i A_i \sin(\ln_i \cdot \mathbf{r}) + \sum_i B_i \cos(\ln_i \cdot \mathbf{r}), \quad (8.1)$$

where A_i and B_i are constants and \mathbf{n}_i represents a sequence of unit vectors in the x, y plane.

The triangular and hexagonal patterns (6.2) and (7.1) are applications of this general expression.

The concentric pattern of section 5 is also derived from expression (8.1) replacing the summation by an integration over a continuous set of unit vectors distributed with equal weight in all horizontal directions. The procedure is readily generalized to a noncircular pattern by adding a weight-factor function of the orientation. For example, an elliptic pattern may be derived quite simply.

Very general periodic patterns are obtained by introducing the requirement of periodicity of expression (8.1) in given directions. For example, if the pattern (8.1) has a period whose magnitude and direction is defined by the vector \mathbf{a} the pattern must remain unchanged under a translation \mathbf{a} . This requires the condition that for all vectors \mathbf{n}_i it is possible to write

$$\ln_i \cdot \mathbf{a} = 2\pi k_i, \quad (8.2)$$

where k_i is any positive or negative integer or zero. With a unit vector \mathbf{n}_a in the direction of \mathbf{a} and with a denoting the absolute magnitude of \mathbf{a} , we write

$$\mathbf{n}_i \cdot \mathbf{n}_a = \frac{2\pi}{la} k_i. \quad (8.3)$$

This result is equivalent to stating that the projections of the vectors \mathbf{n}_i on the direction of \mathbf{a} are all commensurable.

The pattern may also be required to be periodic in another direction of vector period \mathbf{b} . We shall then require a similar condition that the projections on the \mathbf{b} direction of the vectors \mathbf{n}_i be commensurable.

In particular the triangular pattern (6.2) may be generalized by writing

$$w(x, y) = \sin(\mathbf{l}\mathbf{n}_1 \cdot \mathbf{r} + \theta) + \sin(\mathbf{l}\mathbf{n}_2 \cdot \mathbf{r} + \theta) + \sin(\mathbf{l}\mathbf{n}_3 \cdot \mathbf{r} + \theta), \quad (8.4)$$

where the unit vectors $\mathbf{n}_1, \mathbf{n}_2, \mathbf{n}_3$ are again oriented at 120 degrees from each other as in Figure 4. The pattern is periodic and has the symmetry of the equilateral triangle. For $\theta=0$ and $\theta=\pi/2$ expression (8.4) yields, respectively, the triangular and hexagonal patterns of Figures 5 and 7. Actually the hexagonal pattern is already obtained for $\theta=\pi/6$. This can be verified by translating expression (7.1) through a distance $x=2\mathcal{L}/3$ in the x direction. When $0 < \theta < \pi/6$ we obtain a continuous series of intermediate cases which we shall refer to as *triangular-hexagonal* patterns. The significance of this result is illustrated by considering the point P of intersection of the crest lines of two of the sinusoidal components. The various triangular-hexagonal patterns are obtained by varying the distance at which the crest line of the third component lies from the intersection P .

In order to obtain a more accurate picture of the pattern we shall apply, as previously, the trigonometric identity (6.3). By putting

$$-X_i = \frac{1}{2}\mathbf{l}\mathbf{n}_i \cdot \mathbf{r} - \theta, \quad (8.5)$$

we may write expression (8.4) as

$$w(x, y) = -4 \sin\left(\frac{1}{2}\mathbf{l}\mathbf{n}_1 \cdot \mathbf{r} - \theta\right) \cdot \sin\left(\frac{1}{2}\mathbf{l}\mathbf{n}_2 \cdot \mathbf{r} - \theta\right) \cdot \sin\left(\frac{1}{2}\mathbf{l}\mathbf{n}_3 \cdot \mathbf{r} - \theta\right) + \sin 3\theta. \quad (8.6)$$

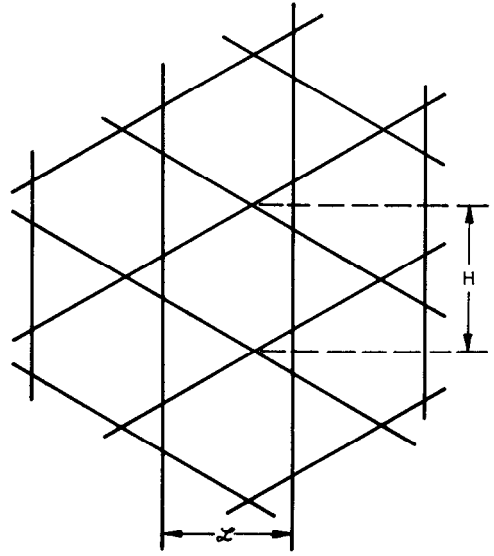


FIG 8. Triangular-hexagonal pattern. Network of contour lines of elevation $w = \sin 3\theta$.

Contour lines for the altitude $w = \sin 3\theta$ constitute a network of straight lines as illustrated in Figure 8. This corresponds to the two triangular-hexagonal patterns shown in Figures 9a and 9b. One is obtained from the other by a change in sign of w .

The pattern is also divided in hexagonal cells. The size of these cells and the distance, H , between peaks is the same as for the triangular and hexagonal patterns of Figures 5 and 7.

Periodic patterns with nonregular hexagonal cells were also obtained by Vernotte (1936). They may be derived as a particular case of the general expression (8.1).

9. TIME-HISTORY OF THREE-DIMENSIONAL STRUCTURES

In the previous discussion we have considered patterns derived from two-dimensional solutions with the same wavelength in all directions. In practice the unstable pattern which will emerge after a sufficient time will correspond to the dominant wavelength of the two-dimensional solution.

However, as we have seen there are an infinite number of three-dimensional patterns which have the same rate of growth and correspond to the same dominant wavelength. The particular pattern which will emerge depends on irregularities initially present in the layered structure. For example, if the structure is composed of a number of homogeneous fluid layers of different densities

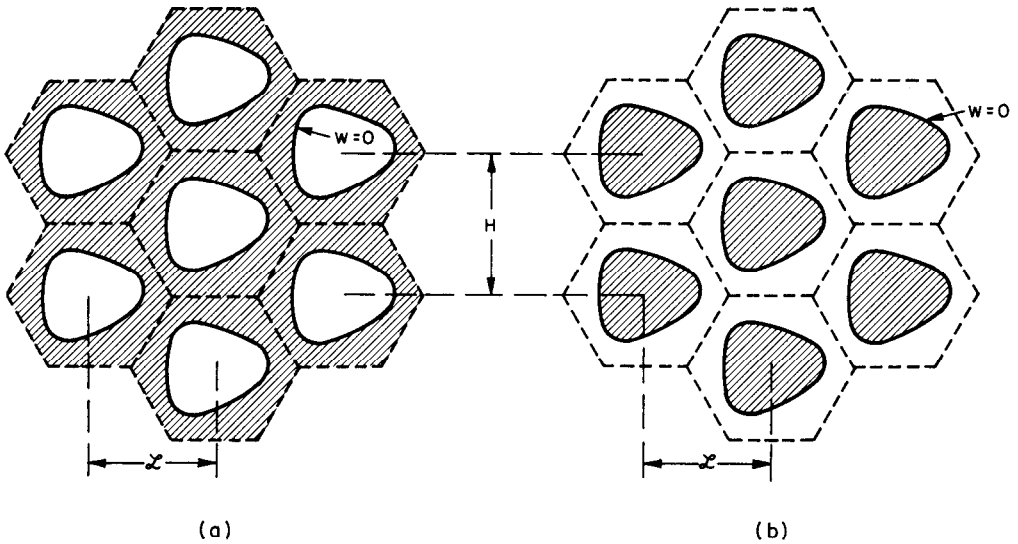


FIG. 9. Triangular-hexagonal patterns showing nodal lines and hexagonal cells. Characteristic distance between peaks is $H = 1.155\mathcal{L}$.

the initial irregularities are represented by the initial deviation of each interface from a perfect horizontal plane. In geological structures such derivations may be due to tectonic forces or uneven sedimentation.

The time-history of the unstable deformation for such initial conditions may be obtained from the basic two-dimensional solution by the following somewhat elaborate but straightforward process.

We first consider the time-history of a sinusoidal two-dimensional solution with initial conditions such that all interfaces except one are different from a perfect horizontal plane at $t=0$. The wavelength $\mathcal{L} = 2\pi/l$ is given. It is a simple matter to solve this problem, by representing the initial deviations of the discontinuity surfaces as a superposition of normal modes of the two-dimensional problem. These modes correspond to characteristic roots for p in the exponential factor $\exp(pt)$.

The degree of the characteristic equation for p is equal to the number N of nonrigid interfaces including the free surface. This means that the plot $p(l)$ of p as a function of l is represented by N branches.

$$p_j = p_j(l) \quad (j = 1, 2, \dots, N). \quad (9.1)$$

There are N modes corresponding to these values. For two-dimensional solutions they are of the form (3.1) and the vertical displacement is written

$$W^{(j)} = f^{(j)}(l, z)e^{p_j t} \cos lx. \quad (9.2)$$

The vertical distribution is written $f^{(j)}(l, z)$ to indicate explicitly that it depends on the wavelength and is different for each mode. The roots $p_j(l)$ may be positive or negative corresponding to either unstable or decaying modes.

The vertical deflections may be represented as a sum of modes

$$W = \sum_{j=1}^N f^{(j)}(l, z)e^{p_j t} \cos lx. \quad (9.3)$$

The vertical displacement at the k th interface of altitude z_k may be written

$$W_k = F_k(l, t) \cos lx, \quad (9.4)$$

with

$$F_k(l, t) = \sum_{j=1}^N f^{(j)}(l, z_k)e^{p_j t}. \quad (9.5)$$

Now each mode, hence each function $f^{(j)}$, contains an arbitrary amplitude factor. These N arbitrary constants may be adjusted so that²

² The constants are conveniently derived by a standard procedure using the orthogonality property

$$\sum_{k=1}^N \Delta\rho_k f^{(\mu)}(l, z_k) f^{(\nu)}(l, z_k) = 0$$

for $\mu \neq \nu$ and $\Delta\rho_k$ = the density discontinuity. This orthogonality condition is a direct consequence of the analog model formulation (Biot, 1965a, page 475).

$$F_k(l, 0) = \begin{cases} 0 & k \neq m \\ 1 & k = m. \end{cases} \quad (9.6)$$

This means that the initial vertical displacement (9.4) is zero except for the m th interface where it is equal to $\cos lx$.

In the value (9.4) we may, of course, replace the factor $\cos lx$ by $\sin lx$ or $\exp(ilx)$ and write W_k in the complex form

$$W_k = F_k(l, t)e^{ilx}. \quad (9.7)$$

By rotation through an angle, α , about the vertical axis it becomes

$$W_k = F_k(l, t)e^{i(\xi x + \eta y)}, \quad (9.8)$$

where ξ and η are the value (3.7) and

$$l = \sqrt{\xi^2 + \eta^2}. \quad (9.9)$$

We shall now determine the time-history of deformation of the various interfaces. We denote by $w_k(x, y, t)$ the vertical displacement of the k th interface as a function of x, y , and t . As initial conditions we assume that $w_m(x, y, 0)$ is given for $k = m$ and is zero for all other interfaces. We express the initial deflection as a double Fourier integral,³

$$w_m(x, y, 0) = \frac{1}{2\pi} \int_{-\infty}^{+\infty} \int_{-\infty}^{+\infty} \phi(\xi, \eta) e^{i(\xi x + \eta y)} d\xi d\eta, \quad (9.10)$$

where

$$\phi(\xi, \eta) = \frac{1}{2\pi} \int_{-\infty}^{+\infty} \int_{-\infty}^{+\infty} w_m(x, y, 0) \cdot e^{-i(\xi x + \eta y)} dx dy. \quad (9.11)$$

Expression (9.10) represents the initial deformation as a super-position of two-dimensional solutions of the type (9.8). Hence, after a time t the vertical displacement of the k th interface is

$$w_k(x, y, t) = \frac{1}{2\pi} \int_{-\infty}^{+\infty} \int_{-\infty}^{+\infty} F_k(l, t) \phi(\xi, \eta) \cdot e^{i(\xi x + \eta y)} d\xi d\eta. \quad (9.12)$$

It is obtained by introducing the factor $F_k(l, t)$ in the integrand of (9.10). This result also yields

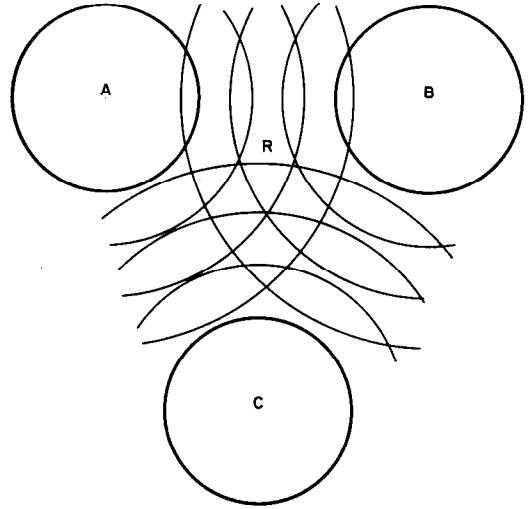


FIG. 10. Dominant three-dimensional pattern due to initial conditions corresponding to slight hills centered at A, B, C .

the time-history when the initial deformation of all interfaces is different from zero by adding the values (9.12) for each interface.

It is possible to obtain some idea of the dependence of the dominant pattern upon initial conditions by a simple reasoning which does not require any calculations. Assume that the initial deformation of the interface is represented by three slight hills centered at A, B , and C (Figure 10). Under unstable conditions each hill will generate a concentric pattern which intersects in the region R . In that region we may therefore expect to observe approximately hexagonal cells with the various inside patterns illustrated in Figures 5, 7, and 9, depending on the phasing of the three intersecting components.

The size of the hexagonal cell, hence the characteristic distance between peaks, as given by expression (6.10), is

$$H = 1.155 \mathcal{L}_d, \quad (9.13)$$

where \mathcal{L}_d is the dominant wavelength of the two-dimensional solution. In regions close to a pair of initial hills the pattern will correspond to approximately rectangular cells whose size corresponds to expressions (4.5) and (4.7) and is equal or very close to the dominant wavelength of the two-dimensional solution.

Note that the initial deviations from a perfect horizontal plane may be represented either by

³ See, for example, Sneddon's book (1951), page 43.

hills and hollows or a combination of both with various amplitudes. This simply changes the phasing and amplitudes of the sinusoidal components and results in a three-dimensional structure with the same general characteristics as those illustrated above.

10. THREE-DIMENSIONAL SALT STRUCTURES WITH VARIABLE OVERBURDEN AND COMPACTION

Due to the linearity of the general problem the present method of superposition of two-dimensional solutions is applicable to the case of three-dimensional instability of salt structures when account is taken of the rate of sedimentation and compaction of the overburden.

The two-dimensional problem was solved in a previous paper (Biot and Odé, 1965) for a layer of salt of given thickness lying on a rigid base. The overburden thickness varies with time at a uniform rate while the density *depends on both time and depth* so as to take into account the non-uniform compaction. The time required for a given amplification of an initial sinusoidal disturbance was plotted as a function of the wavelength in Figure 11 of a previous paper (Biot and Odé, 1965). The value of the dominant wavelength is derived.

By superposition of such two-dimensional solutions we derive the three-dimensional structures for this case corresponding to the square, concentric, triangular, and hexagonal patterns discussed above. This yields the time-history and the distance between peaks and ridges for these various patterns.

These characteristic distances are given by expressions (4.7), (5.8), and (6.10) in terms of the dominant wavelength, \mathcal{L}_d , of the two-dimensional solution. They are not significantly different from \mathcal{L}_d . Previous conclusions regarding the geological validity of the theory as derived from the two-dimensional analysis are therefore applicable to three-dimensional structures with variable overburden.

REFERENCES

- Arrhenius, S., 1912, Zur Physik der Salzlagerstätten: Medd. Vetenskaps akad. Nobelinstit. v. 2, p. 1-25.
- Bénard, H., 1900, Les tourbillons cellulaires dans une nappe liquide: Revue Générale des Sciences Pures et Appliquées, v. 11, p. 1261-1271 and p. 1309-1328.
- 1901, Les tourbillons cellulaires dans une nappe liquide transportant de la chaleur par convection en régime permanent: Annales de Chimie et de Physique, v. 23, p. 62-144.
- Biot, M. A., 1959, The influence of gravity on the folding of a layered viscoelastic medium under compression: Journal of the Franklin Institute, v. 267, p. 211-228.
- 1960, Instability of a continuously inhomogeneous viscoelastic half-space under initial stress: Journal of the Franklin Institute, v. 270, p. 190-201.
- 1961, Theory of folding of stratified viscoelastic media and its implication in tectonics and orogenesis: Geol. Soc. America Bull., v. 72, p. 1595-1620.
- 1963, Stability of multilayered continua including the effect of gravity and viscoelasticity, Journal of the Franklin Institute, v. 276, p. 231-252.
- 1965a, Mechanics of incremental deformations: New York, John Wiley & Sons, Inc., 504 p.
- 1965b, Theory of viscous buckling and gravity instability of multilayers with large deformation: Geol. Soc. America Bull. v. 76, p. 371-378.
- and Odé, H., 1965, Theory of gravity instability with variable overburden and compaction: Geophysics, v. 30, p. 213-227.
- Bisshopp, F. E., 1960, On two-dimensional cell patterns: Journal of Mathematical Analysis and Applications, v. 1, p. 373-385.
- Chandrasekhar, S., 1961, Hydrodynamic and hydro-magnetic stability: Oxford at the Clarendon Press (p. 43-75), 692 p.
- Christopherson, D. G., 1940, Note on the vibration of membranes: Quarterly Journal of Mathematics (Oxford Series), v. 11, p. 63-65.
- Daneš, Z. F., 1964, Mathematical formulation of salt-dome dynamics: Geophysics, v. 29, p. 414-424.
- Dobrin, M. B., 1941, Some quantitative experiments on a fluid salt-dome model and their geological implications: Trans. A.G.U., part 2, p. 528-542.
- Hubbert, M. King, 1937, Theory of scale models as applied to the study of geological structures: Geol. Soc. America Bull., v. 48, p. 1459-1520.
- McLachlan, N. W., 1934, Bessel functions for engineers: Oxford Clarendon Press, 192 p.
- Nettleton, L. L., 1955, History of concepts of Gulf Coast salt-dome formation: Bull. A.A.P.G., v. 39, p. 2373-2383.
- Parker, T. J., and McDowell, A. N., 1955, Model studies of salt-dome tectonics: Bull. A.A.P.G., v. 39, p. 2384-2470.
- Lord Rayleigh, 1916, On the convection currents in a horizontal layer of fluid when the higher temperature is on the under side: Phil. Mag., v. 32, p. 529-546. (Also Scientific Papers, v. 6, p. 432-446, Cambridge, England, 1920.)
- Sneddon, I. N., 1951, Fourier transforms: New York, McGraw Hill Book Company, Inc., 542 p.
- Vernotte, P., 1936, Les dimensions théoriques des tourbillons cellulaires de Bénard: Comptes rendus, v. 202, p. 1764-1767, v. 203, p. 43-46, and v. 203, p. 985-987. (The problem is also discussed in a book by the same author, Thermocinétique: Publications Scientifiques et Techniques du Ministère de l'Air, Paris, 1949.)